**Supplemental Materials:**
Supplemental Figure Tables and Legends

SUPPLEMENTAL TABLE 1: Ssec and pvalue of permutation score for each top-ranked peptide, related to Figure 2

SUPPL FIG 1 – PERMUTATION TESTING AND OVERVIEW FIGURE

SUPPL FIG 2 – BIOGPS ARRAYS USED TO INFER TISSUE SPECIFICITY

SUPPL FIG 3 – SEX DIFFERENCES AMONG SSEC SCORES

SUPPL FIG 4 – ALTERNATIVE STRATEGIES TO CROSS-TISSUE CORRELATIONS

SUPPL FIG 5 – QQPLOTS FOR ENRICHMENT OF SECRETED FACTORS

SUPPL FIG 6 - LCN5 DOSE-DEPENDENT TREATMENT

SUPPL FIG 7 – LCN5 MRNA QUANTIFICATION IN COCULTURED MYOTUBES

SUPPL FIG 8 – PLASMA ADENO PROTEIN MEASUREMENTS

SUPPL FIG 9 – ADENO-LCN5 MICE ON NORMAL CHOW DIET ITT AND GTT

SUPPL FIG 10 – AAV-LCN5 COHORT EXPREIMENTS

SUPPL FIG 11 – TISSUE-WIDE GFP BLOTS TO ASSESS LCN5 TARGETS

SUPPL FIG 12 – CONCORDANCE OF SSEC BETWEEN HMDP AND STARTNET

SUPPL FIG 13 – NOTUM POOLED EXPERIMENT METABOLIC CAGE MEASUREMENTS

# SUPPLEMENTARY MATERIAL

## SUPPLEMENTARY FIGURE LEGENDS

SUPPL FIG 1 – PERMUTATION TESTING AND OVERVIEW FIGURE, related to Figure 2: An overview2 of the $S_{sec}$ calculation is outlined starting with expression arrays from 2 tissues. In addition, we not the permutation tests with a green arrow on the right. Here, the observed $S_{sec}$ score is tested against datasets with permuted target tissue strain expression. An example for the permutation for the top-ranked adipose-to-muscle gene is shown.

SUPPL FIG 2 – BIOGPS ARRAYS USED TO INFER TISSUE SPECIFICITY, related to Figure 4A and Figure 7A: BioGPS array data showing the tissue-wide expression of Lcn5 (**A**) and Notum (**B**).

SUPPL FIG 3 – SEX DIFFERENCES AMONG SSEC SCORES, related to Figure 2: For adipose and liver HMDP expression, $S_{sec}$ was performed on sex and tissue-specific circuits. Plotted are the correlations between sexes of the relative $S_{sec}$ ranking for all secreted proteins (**A, B**) or the 50 highest-ranked (**C, D**). We note very strong concordance of correlation with all genes, but significantly less when focusing on the top 50, which are inferred to represent the strongest axes of communication.

SUPPL FIG 4 – ALTERNATIVE STRATEGIES TO CROSS-TISSUE CORRELATIONS, related to Figure 1 and Figure 2: For the two cross-tissue circuits explored in detail, we are plotting the correlations of ranking for each protein derived from either $S_{sec}$ or various pvalue cut-offs. Adipose-to-muscle is shown on top and liver-to-adipose on bottom. Since the correlations are particularly strong and, therefore, many genes overlap, a density count was included. The density count reflects the number of genes within a given spatial region to allow color representation overlapping values. We observe highly significant similarities amongst the

various ranking strategies for cross-tissue correlation, as evident by the indicated correlation coefficents and pvalues.

SUPPL FIG 5 – QQPLOTS FOR ENRICHMENT OF SECRETED FACTORS, related to Figure 1: For each cross-tissue axis in **Fig 2**, qqplots were generated by comparing cross-tissue $S_{sec}$ scores for secreted proteins (y-axis) vs genes coding for non-secreted proteins (x-axis). Script used to generate QQ-Plots is also provided in the Github. To show this relationship, the sum of -ln(pvalue) was determined for all non-secreted factors, which when correlated against themselves on a scatterplot, producing the red line of perfect correlation. Next, secreted factors values were superimposed, where the y-axis position determined by the sum of -ln(pvalue) across target tissue transcripts and x-axis value were matched for bins of percentile based on the relative rank of correlation, corresponding to rankings between secreted and non-secreted factors. The relative ranking was used since the number of secreted vs non-secreted factors varied depending on tissue and mode of detection (type of array or RNA-sequencing). Differences in numbers of genes detected in each tissue is also the reason why the axes of each cross-tissue comparison show somewhat differing values for their distribution. For example, the muscle-to-adipose tissue y-axis possesses a higher numeric range due to the combination of more genes detected in muscle, as well as the strong cross-tissue correlation of non-secreted factors specific for this axis. Given that the sum of the -ln(pvalue) is directly proportional to the Ssec score, regardless of the range shown below each axis, the interpretation of the enrichment of secreted vs non-secreted factors remains constant for every comparison. Most cross-tissue axes show enrichment for secreted factors at the higher significance levels (top-right region of the graph).

SUPPL FIG 6 - LCN5 DOSE-DEPENDENT TREATMENT, related to Figure 4: C2C12 myotubes were treated overnight (16hrs) with indicated doses of LCN5 then qPCR probed for the genes listed. N=4 All data presented as mean ± SEM *p<0.05, **p<0.01

SUPPL FIG 7 – QUANTIFICATION OF LCN5 IN COCULTURE EXPERIMENTS, related to Figure 4I-K: 3T3L Adipocytes used in Fig 4I-K were quantified for the transcript abundance of Lcn5 using qPCR. N = 4, All data presented as mean ± SEM *p<0.05

SUPPL FIG 8 – PLASMA ADENO PROTEIN MEASUREMENTS, related to Figure 5: Western blots ad corresponding quantifications for plasma measurements of Ad-LCN5 (A), Ad-NOTUM (B).

SUPPL FIG 9 – ADENO-LCN5 MICE ON NORMAL CHOW DIET ITT AND GTT, related to Figure 5: Mice administered Ad-GFP or Ad-LCN5 for 9 days were subjected to an oral glucose or insulin tolerance test, in a similar fashion as in **Fig 5C-F**.

SUPPL FIG 10 – AAV-LCN5 COHORT EXPREIMENTS, related to STAR Methods section *Adeno-associated virus models*: Mice administered AAV-GFP or AAV-LCN5 and HF/HS diet for time-courses indicated were evaluated for body weight, composition, insulin and glucose tolerance.

SUPPL FIG 11 – TISSUE-WIDE GFP BLOTS TO ASSESS LCN5 TARGETS, related to Figure 4I-K and Figure 5: Indicated tissues from mice in Suppl. Fig. 10 were immuoprobed for GFP to identify target tissues of LCN5. Below the same Plantaris and Soleus muscles were immuoprobed for Noq7 to verify fiber type.

SUPPL FIG 12 – CONCORDANCE OF SSEC BETWEEN HMDP AND STARTNET, related to Figure 6: $S_{sec}$ scores for all matching datasets between the two populations are plotted. The

strategy is presented in A and data points in B, where r, and pvalues indicated significant concordance.

SUPPL FIG 13 – NOTUM POOLED EXPERIMENTS FOR METABOLIC CAGES, related to Figure7: Pooled replicates from 3 experiments of metabolic chambers from mice administered Ad-GFP or Ad-NOTUM aggregated (**A-F**) or presented as time-series data (**G, H**)

SUPPL FIG 1 – PERMUTATION TESTING AND OVERVIEW FIGURE:

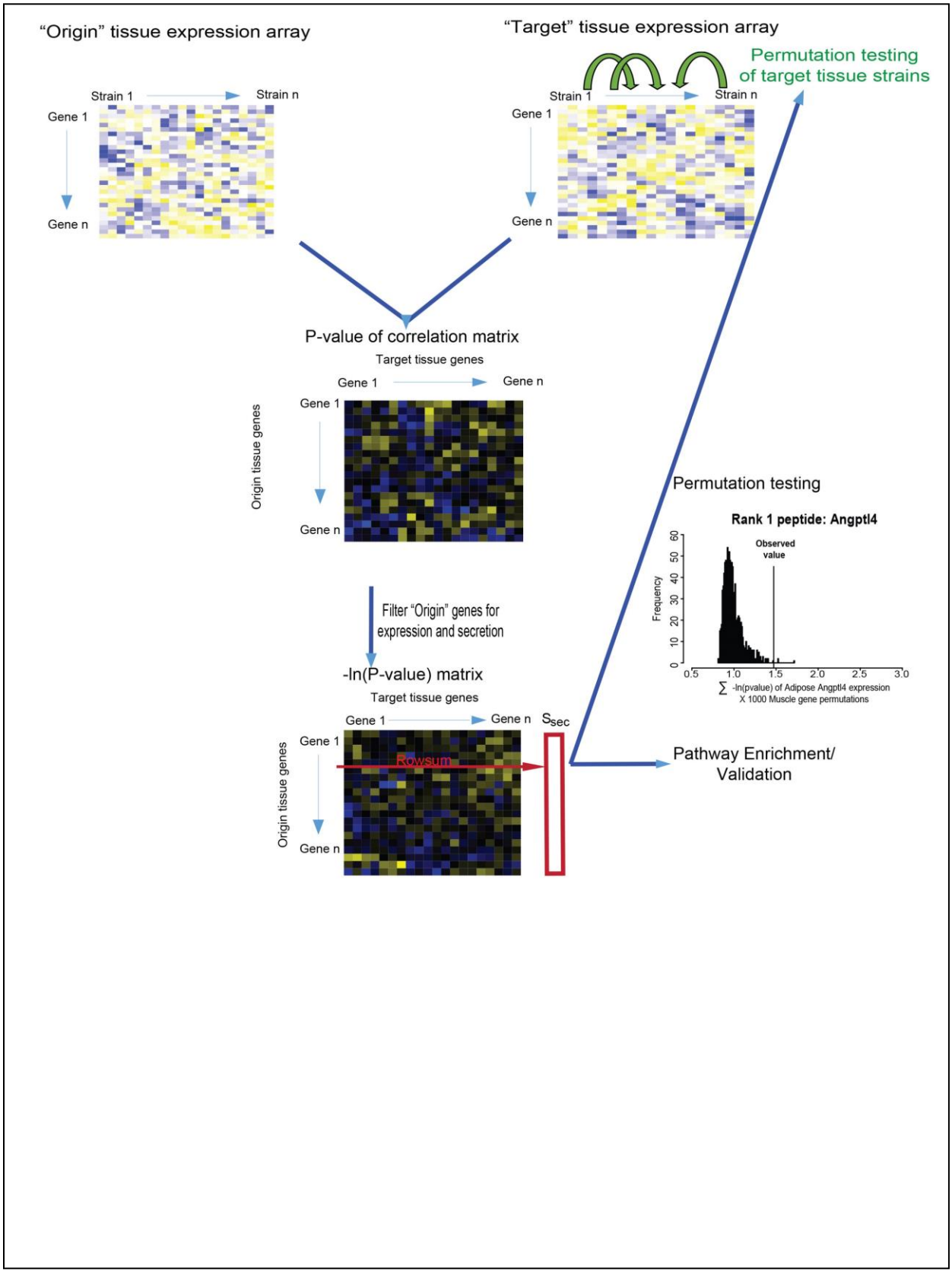

SUPPL FIG 2 – BIOGPS ARRAYS USED TO INFER TISSUE SPECIFICITY

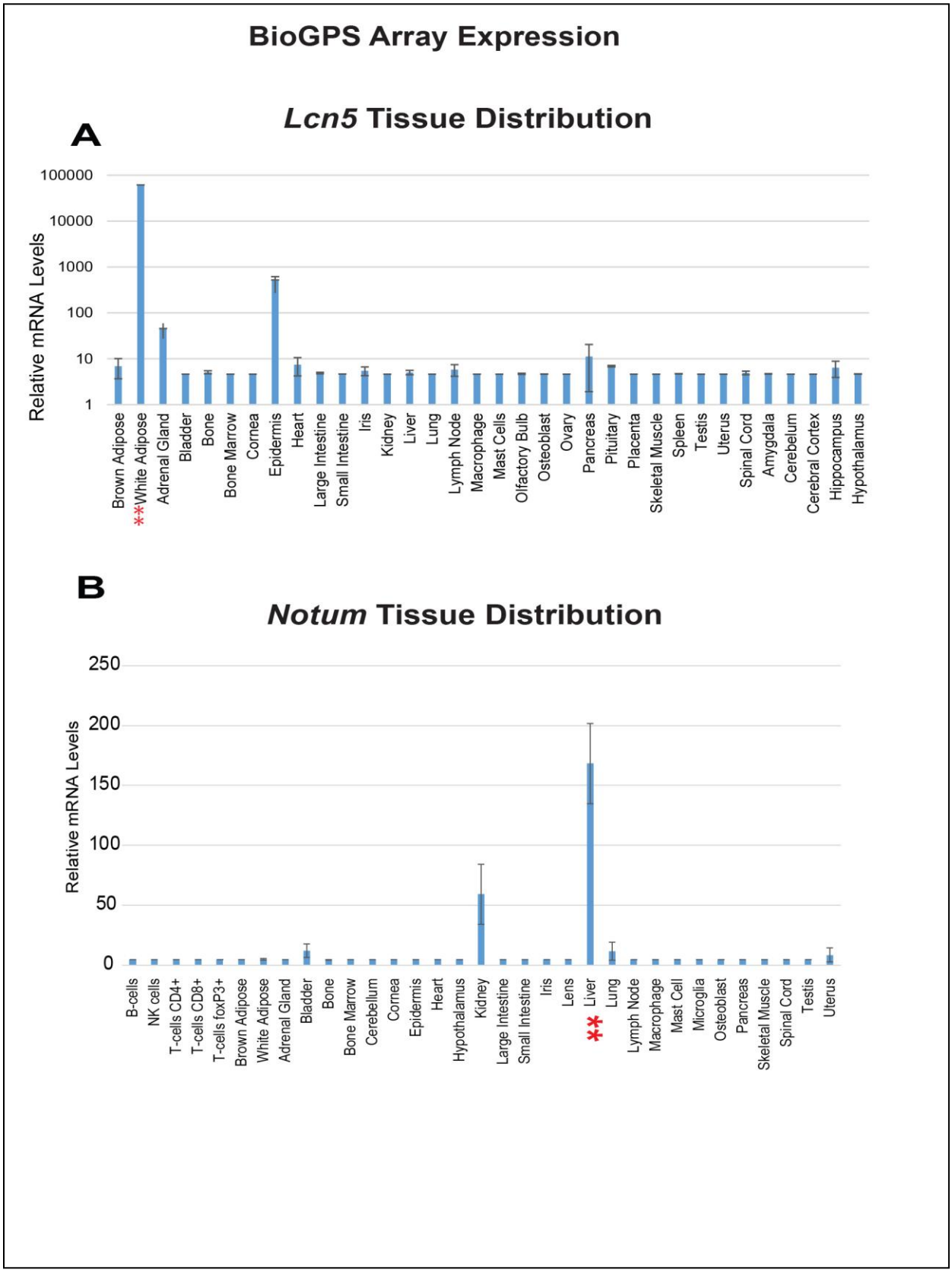

SUPPL FIG 3 – SEX DIFFERENCES AMONG SSEC SCORES

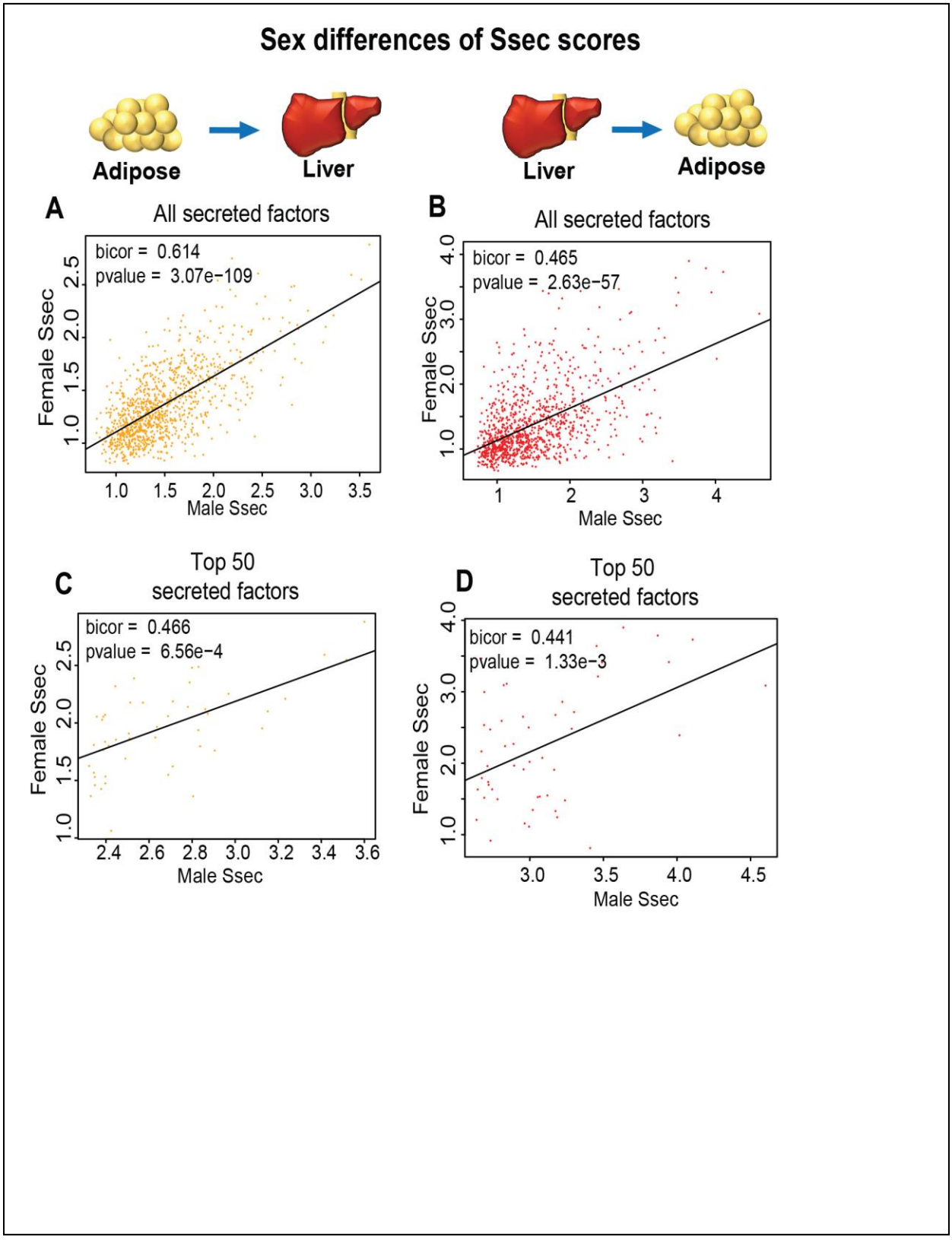

SUPPL FIG 4 – ALTERNATIVE STRATEGIES TO CROSS-TISSUE CORRELATIONS

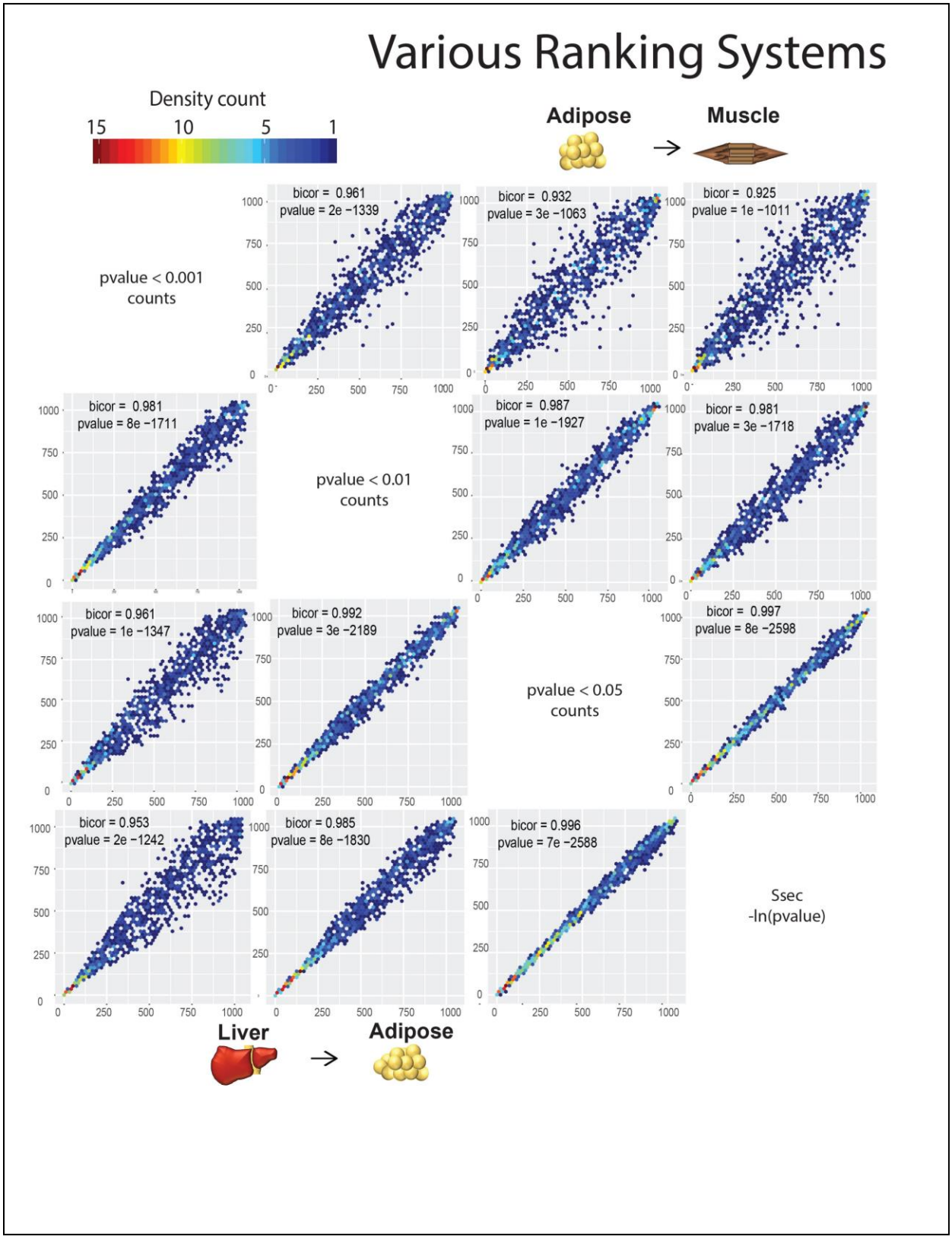

SUPPL FIG 5 – QQPLOTS FOR ENRICHMENT OF SECRETED FACTORS

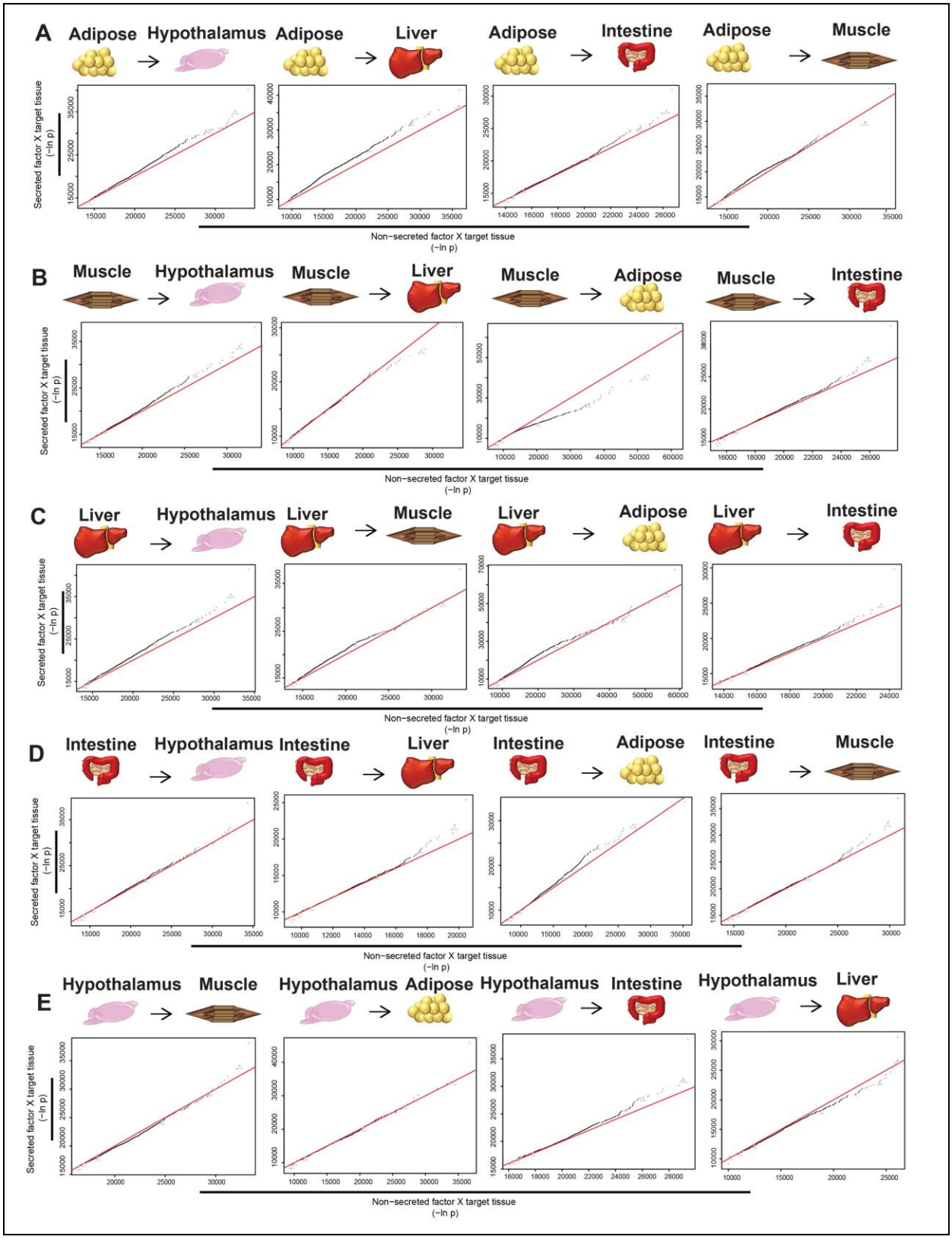

SUPPL FIG 6 - LCN5 DOSE-DEPENDENT TREATMENT

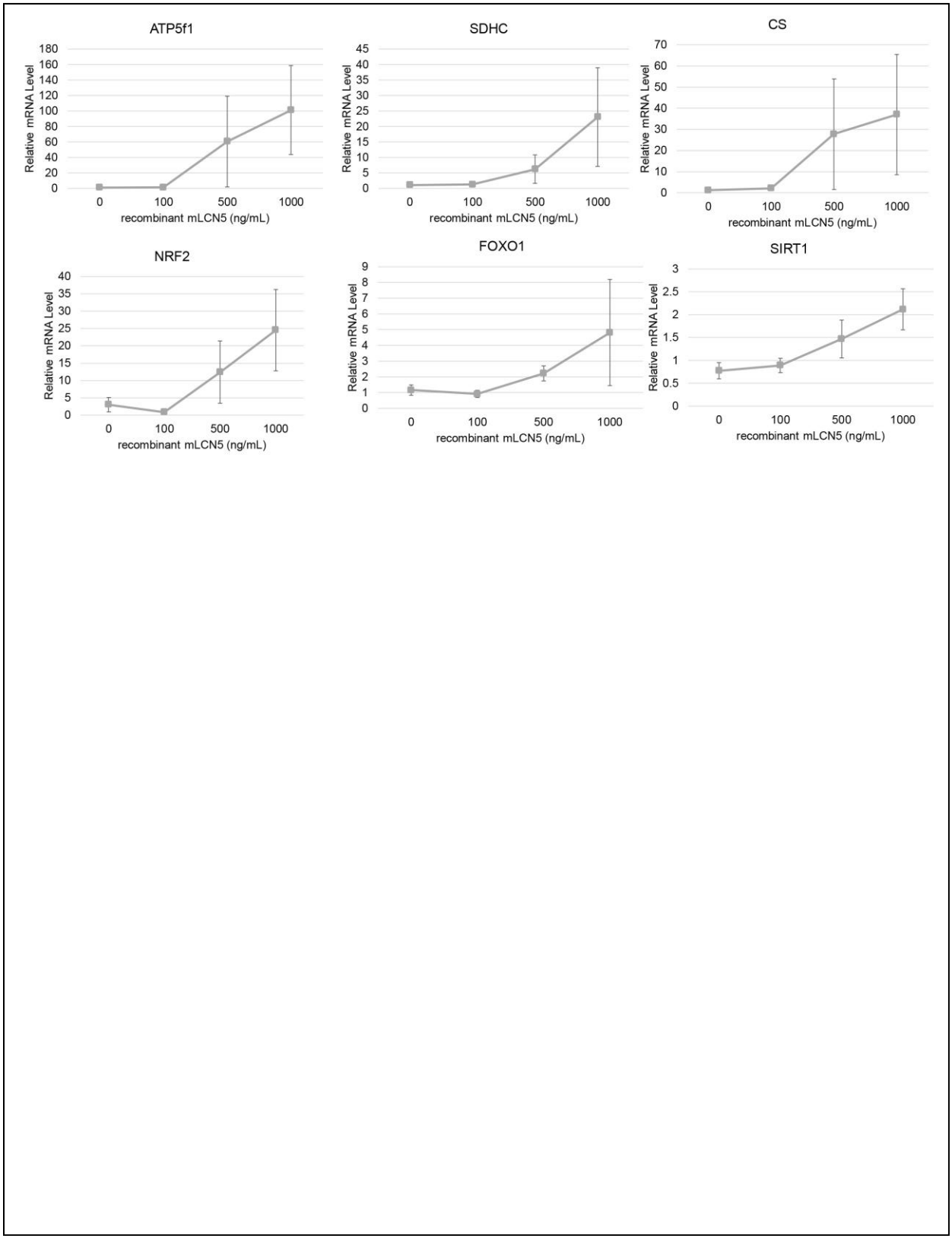

SUPPL FIG 7 – LCN5 MRNA QUANTIFICATION IN COCULTURED MYOTUBES

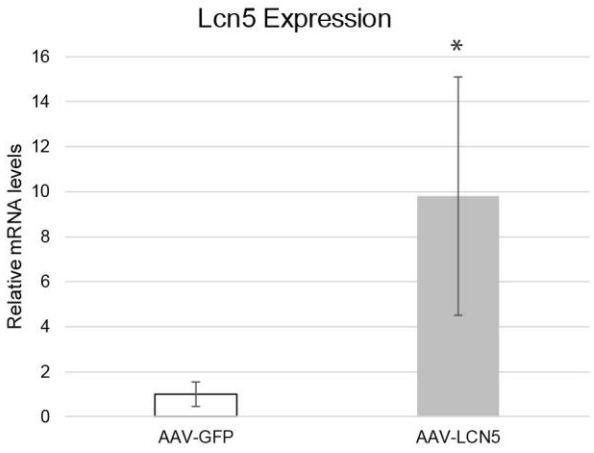

SUPPL FIG 7 – PLASMA ADENO PROTEIN MEASUREMENTS

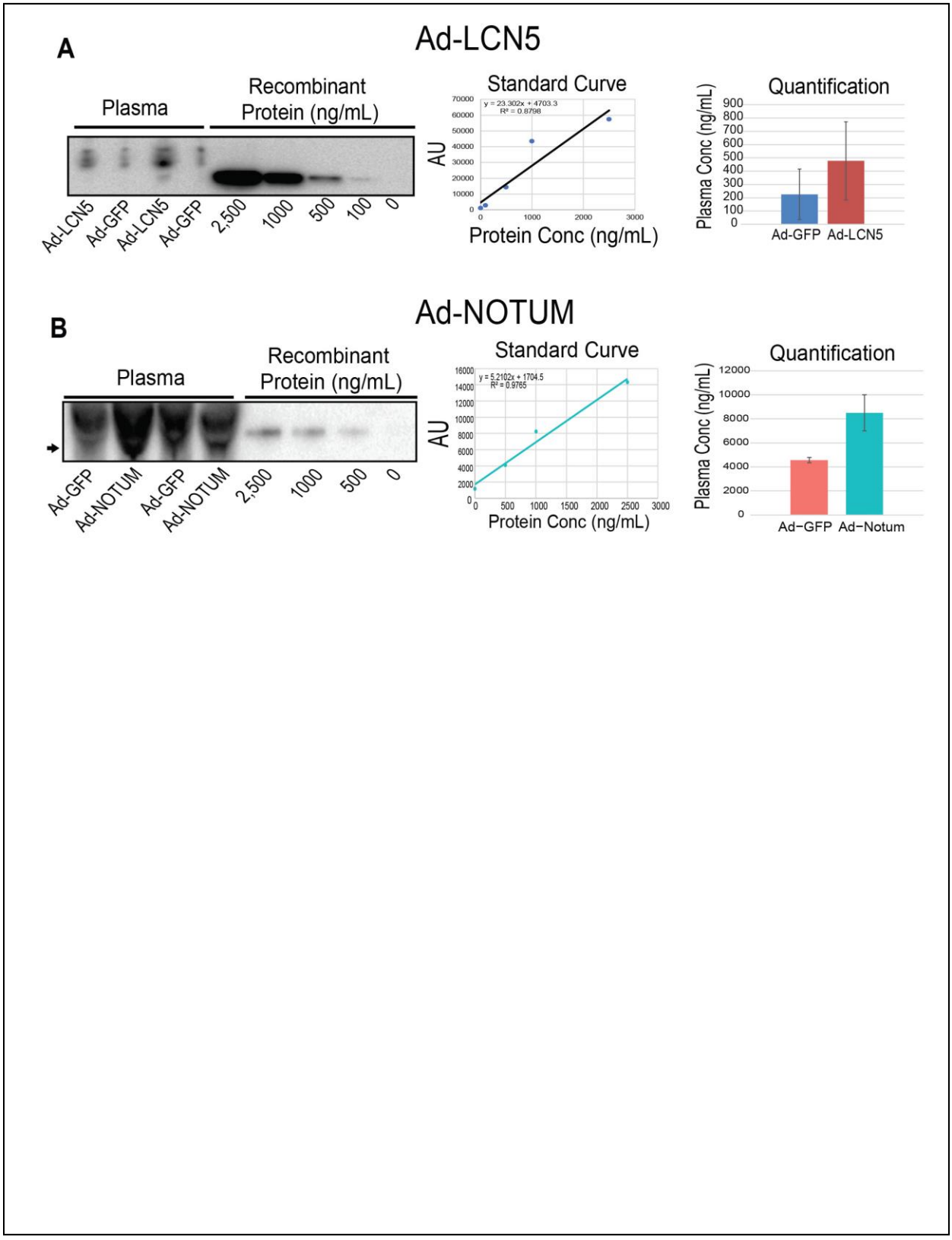

SUPPL FIG 9 – ADENO-LCN5 MICE ON NORMAL CHOW DIET ITT AND GTTSUPPL

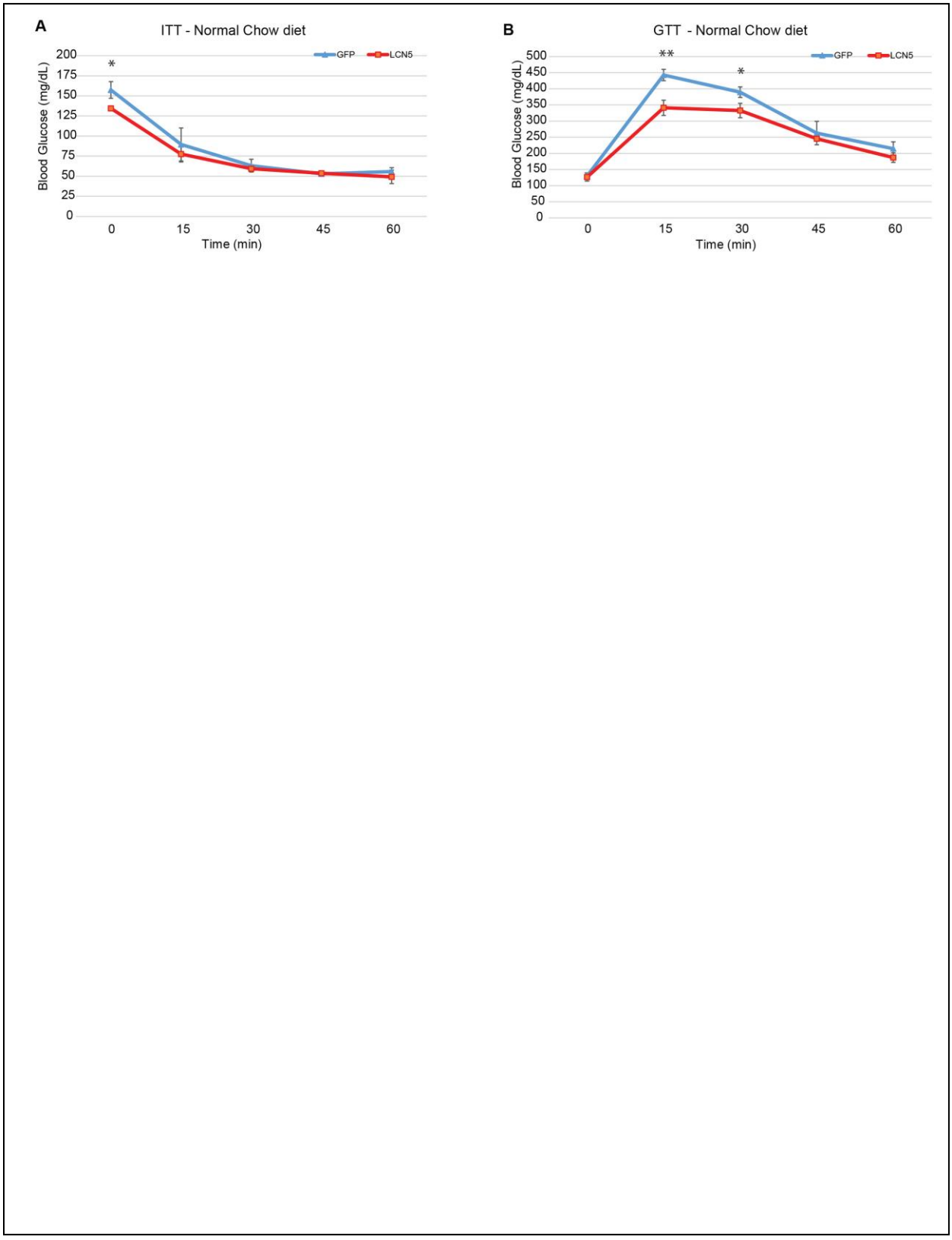

SUPPL FIG 10 – AAV-LCN5 COHORT EXPREIMENTS

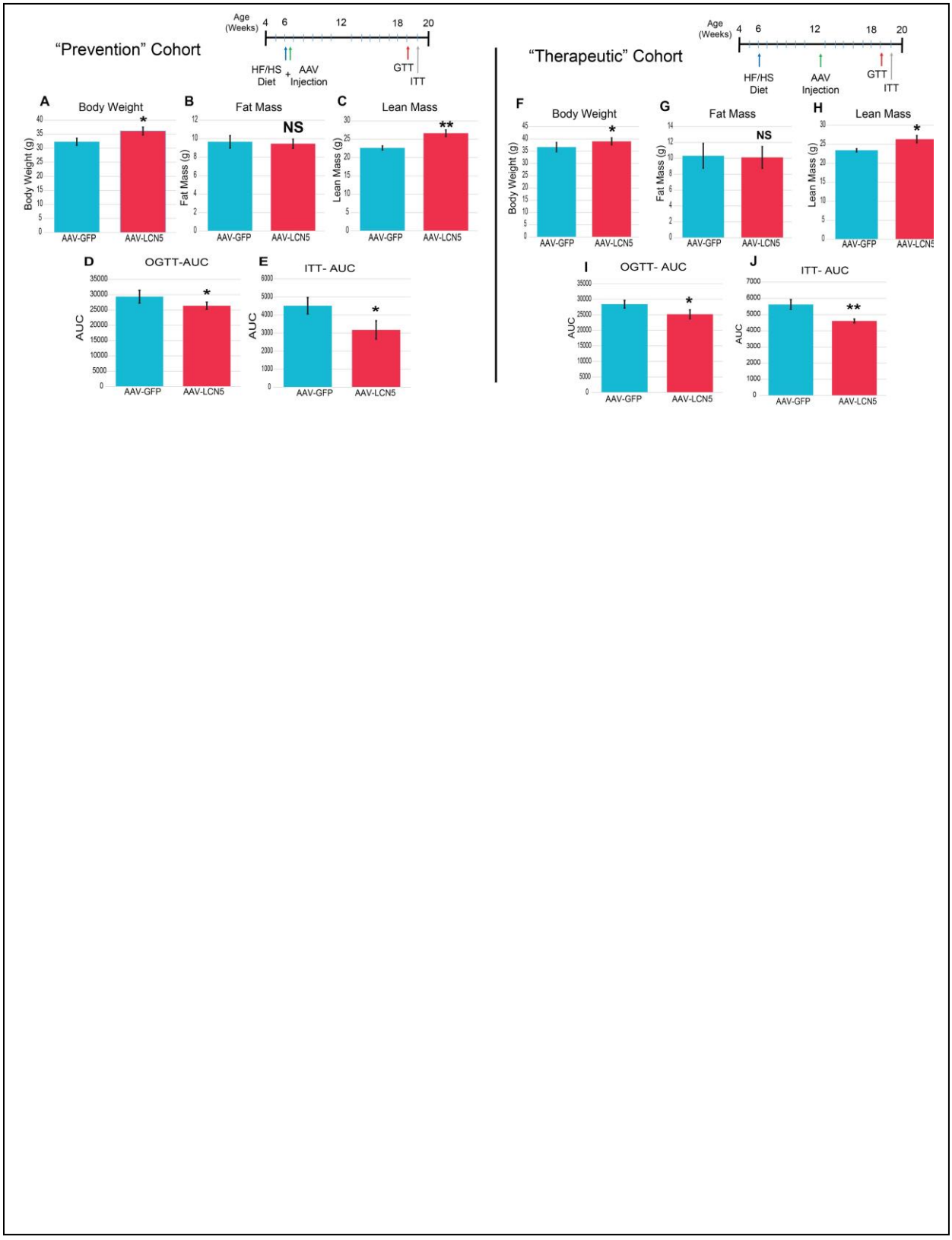

SUPPL FIG 11 – TISSUE-WIDE GFP BLOTS TO ASSESS LCN5 TARGETS

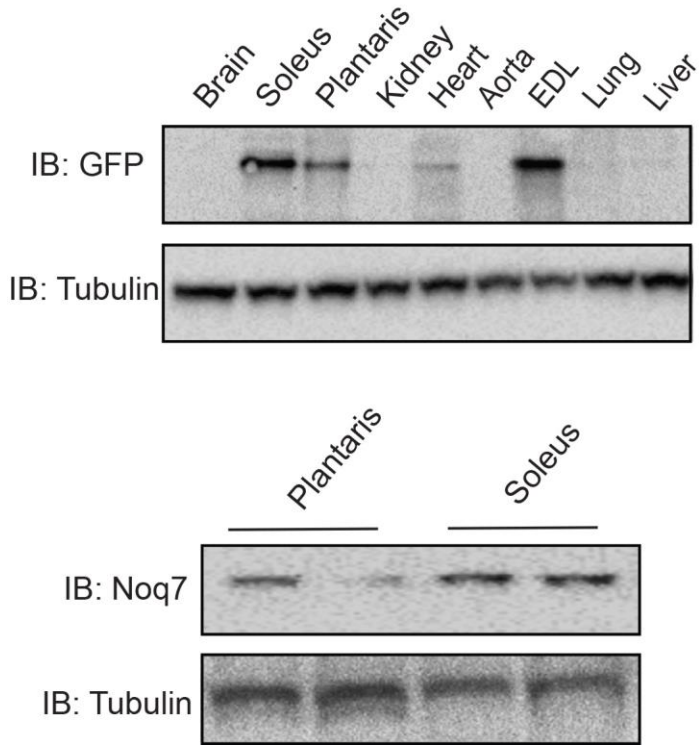

SUPPL FIG 12 – CONCORDANCE OF SSEC BETWEEN HMDP AND STARTNET

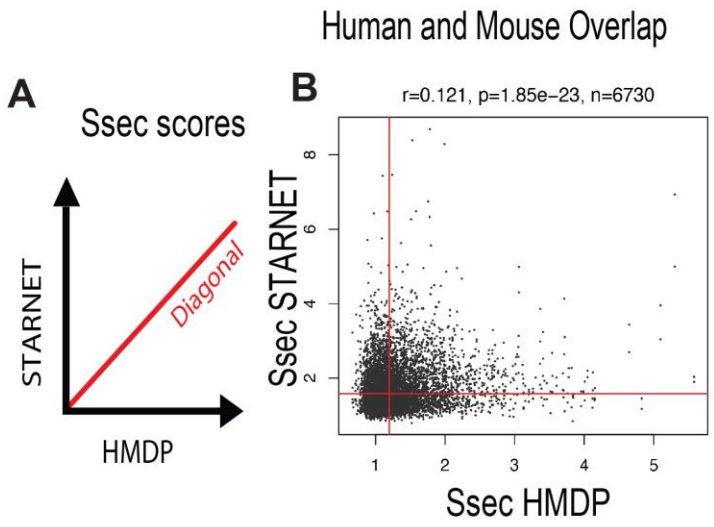

SUPPL FIG 13 – NOTUM POOLED EXPERIMENTS FOR METABOLIC CAGE